Possible crater-based pingos, paleolakes and periglacial landscapes at the high latitudes of Utopia Planitia, Mars

R.J. Soare, Susan J. Conway, G.D. Pearce, J.M. Dohm, P.M. Grindrod

HAL Id: insu-02276063

https://insu.hal.science/insu-02276063

Submitted on 24 Jun 2022

Open Research Online
The Open University's repository of research publications
and other research outputs

Possible crater-based pingos, paleolakes and periglacial landscapes at the high latitudes of Utopia Planitia, Mars

Journal Item

For guidance on citations see FAQs.

oro.open.ac.uk

Accepted Manuscript

Possible crater-based pingos, paleolakes and periglacial landscapes at the high latitudes of Utopia Planitia, Mars

R.J. Soare, S.J. Conway, G.D. Pearce, J.M. Dohm, P.M. Grindrod

1

2

3 **Possible crater-based pingos, paleolakes and periglacial landscapes at**

4 **the high latitudes of Utopia Planitia, Mars**

5

6 R.J. Soare[1], S.J. Conway[2a,b], G.D. Pearce[1], J.M. Dohm[3], P.M. Grindrod[4]

7

8 [1]Department of Geography, Dawson College
9 3040 Sherbrooke Street West, Montreal, Quebec, Canada, H3Z 1A4
10 rsoare@dawsoncollege.qc.ca
11
12 [2a]Department of Physical Sciences, Open University
13 Walton Hall, Milton Keynes
14 UK, MK7 6AA
15 (presently at)
16
17 [2b]LPGN, CNRS/Université Nantes 44322
18 Nantes, France; 3 UMR 8148
19 (work done at)
20
21 [3]Department of Hydrology & Water Resources
22 University of Arizona, USA, 85721
23
24 [4]Department of Earth Sciences, University College, London
25 Gower Street, London, UK. WC1E 6BT
26
27

28

29

30

31 **Pages:** 28

32 **Figs:** 13 (including a supplementary figure)

33 **Tables:** 2

34 *Abstract*

35   Closed-system pingos (CSPs) are perennial ice-cored mounds that evolve in relatively

36 deep and continuous permafrost. They occur where thermokarst lakes either have lost or are

37 losing their water by drainage, evaporation or sublimation and form by means of freeze-thaw

38 cycling, permafrost aggradation and pore-water migration. The presence of CSPs on Mars,

39 particularly on late-Amazonian Epoch terrain at near-polar latitudes, would indicate: 1. the

40 antecedent occurrence of ponded water at the mound-formation sites; 2. freeze-thaw cycling of

41 this water; and, 3. boundary-conditions of pressure and temperature at or above the triple point of

42 water much more recently and further to the north than has been thought possible.

43   In 2005 we studied two crater-floor landscapes in northern Utopia Planitia and used

44 MOC narrow-angle images to describe mounds within these landscapes that shared a suite of

45 geological characteristics with CSPs on Earth. Here, we show the results of a circum-global

46 search for similar crater-floor landscapes at latitudes > 55°N. The search incorporates all

47 relevant MOC and HiRISE images released since 2005. In addition to the two periglacially

48 suggestive crater-floor landscapes observed by us earlier, we have identified three other crater

49 floors with similar landscapes. Interestingly, each of the five mound-bearing craters occur within

50 a tight latitudinal-band (64-69°N); this could be a marker of periglacial landscape-modification

51 on a regional scale.

52   Just to the north of the crater-based pingo-like mounds Conway et al. (2012) have

53 identified large (km-scale) crater-based perennial ice-domes. They propose that the ice domes

54 develop when regional polar-winds transport and precipitate icy material onto the floor of their

55 host craters. Under a slightly different obliquity-solution ice domes could have accumulated at

56 the lower latitudes where the putative CSPs have been observed. Subsequently, were

57   temperatures to have migrated close to or at 0°C the ice domes could have thawed, forming

58   endogenic paleolakes. This region also contains a significant concentration of crater-floor

59   polygons. The polygons are thought to have formed by desiccation (El Maarry et al., 2010, 2012)

60   or thermal contraction (Soare et al., 2005); on Earth each of these processes is associated with

61   the end-stage of lake evolution.

62   On the basis of our enhanced image collection, a new map displaying the global

63   distribution of mound-bearing craters and a two new digital-elevation models of a crater-floor

64   with pingo-like mounds, we evaluate the CSP hypothesis anew.   We   also   explore   two

65   alternative hypotheses: 1. the mounds are weathered central-uplift complexes; or, 2. they are

66   impact-related hydrothermal structures. However, we propose that the CSP hypothesis is much

67   more   robust   than   these   alternatives,   encompassing   geomorphological,   cartographical,

68   stratigraphical and climatological observations, and less subject to inconsistencies.

69   **Key words:** Mars climate, polar geology, surface

70   *1. Introduction*

71   Closed-system (hydrostatic) pingos (CSPs) are perennial ice-cored hills or mounds. They

72   evolve and persist only in permafrost, i.e. ground that is frozen for periods of no less than two

73   years, that is continuous and relatively deep (Washburn, 1973; Harris et al., 1988; Mackay, 1998;

74   French, 2007). CSPs are tens of metres in height and have basal diameters that reach hundreds of

75   metres in some instances **(Fig. 1)**.Their shape ranges from circular to sub-circular to elongate

76   **(Fig. 1)**. Other landforms such as small-sized polygons ($\leq$ 40m in diameter) **(Fig. 2g)** formed by

77   means of thermal-contraction cracking, and polygon-trough/junction pits, often are observed in

78   close spatial-association with CSPs (Washburn, 1973; Mackay, 1998; French, 2007) **(Fig. 2b)**.

79   On Earth, CSPs occur in regions such as the Tuktoyaktuk Coastlands (TC) of northern

80   Canada where thermokarst lakes either have lost or are losing their water by drainage,

81   evaporation or sublimation (e.g. Harris et al., 1988; Mackay, 1998) **(Figs. 2a-e; f-h)**. They are

82   the product of seasonal freeze-thaw cycling (as are the ice-wedges that underlie the small-sized

83   polygons with which they may be associated spatially), permafrost aggradation and soil-moisture

84   (pore-water) migration (Washburn, 1973; Mackay, 1998; French, 2007).

85   The identification of closed-system pingos on Mars, particularly on late-Amazonian

86   Epoch terrain at or near-polar latitudes would point to: 1. the antecedent occurrence of ponded

87   water at the mound-formation sites; 2. freeze-thaw cycling of this water; and, 3. boundary-

88   conditions of pressure and temperature at or above the triple point of water much more recently

89   and further to the north than many workers have thought possible.

90   In 2005 a small set of narrow-angle MOC (Mars Orbiter Camera, Mars Global Surveyor)

91   images were used to describe two crater-floor landscapes in northern Utopia Planitia (UP) that

92   showed mounds with morphological characteristics and landform associations similar to the

93   CSPs of the TC (Soare et al., 2005a; 2005b). The images covered only a part of the crater floors.

94   Using all relevant HiRISE (Mars Reconnaissance Orbiter, High Resolution Imaging Science

95   Experiment) and MOC images (not available at the time of our earlier work and exhibiting

96   complete crater-floor coverage) we have performed a circum-global search for similar crater-

97   floor landscapes at latitudes > 55°N. Three other crater floors that show similar landscapes have

98   been identified. Interestingly, all of the mound-bearing craters are located within a tight

99   latitudinal-band (64-69°N), centred in northern UP **(Fig. 3, Table 1)**. This could be a marker of

100   landscape-modification on a regional scale.

101   Just to the north of the pingo-like mounds Conway et al. (2012) have identified large

102   (km-scale) crater-based perennial ice-domes in a near-polar latitudinal band (70°N). They

103   propose that the ice domes are the product of regional polar-winds that transport and precipitate

104   icy material onto the floor of their host craters. Under a slightly different obliquity-solution the

105   same process could have occurred further to the south, in those craters where the putative closed-

106   system pingos have been observed. Subsequently, were temperatures to have migrated close to or

107   at 0°C the ice domes could have thawed, forming endogenic paleolakes. This region also

108   contains a significant concentration of crater-floor polygons with diameters ≤ 350m. The

109   polygons are thought to have formed by desiccation (El Maarry et al., 2010, 2012) or thermal

110   contraction (Soare et al., 2005); on Earth, each of these processes is associated with the end-stage

111   of lake evolution.

112   Using an enhanced image collection, a new map displaying the global distribution of

113   mound-bearing craters and two new digital-elevation models of a crater-floor with pingo-like

114   mounds, we evaluate the CSP hypothesis anew. We also explore two alternative hypotheses: 1.

115   the mounds are weathered central-uplift complexes; or, 2. they are impact-related hydrothermal

116   structures.

117   *2. Methods*

118   As noted in the introduction, Soare et al. (2005a, b) employed narrow-angle MOC images

119   (3-6m/pixel) to identify, discuss and map two crater-floor landscapes with putative CSPs in

120   northern UP. At the time, narrow-band and high-resolution image coverage of the study region -

121   55-70°N and   60-120°E - was incomplete. Thus, there were significant gaps in our map and

122   intriguing as the CSP hypothesis appeared to be, its validation was beyond the compass of

123   available data.

124   Now, all of the relevant MOC and HIRISE images of this region that were not available

125   in 2005 are integrated with the more continuous impact-crater data collected by Conway et al.

126   (2012) from MOLA (Mars Orbiter Laser Altimeter, Mars Global Surveyor) coverage. Moreover,

127   we use all available HiRISE images (30-60cm/pixel) to extend the longitudinal reach of our

128   study zone from a regional perspective to a circumpolar one (i.e., from 60^0 of coverage to 360^0).

129   Within this transect all imaged craters exhibiting diameters >7km were inspected for mounds.

130   The depth-diameter data for the craters in the region are derived as follows. Intact crater

131   rims are digitised in MOLA data using the watershed methods detailed in Conway et al. (2012)

132   and from this the centre-points calculated. The crater depths are taken as the lowest point on

133   crater floor to the highest point on the rim according to gridded MOLA data and the diameters

134   are estimated by calculating the average centre-to-rim distance (for more detail see Conway et al.

135   2012).

136   Within each of the mound-bearing craters, all of the mounds are mapped. Where

137   topographic data of the craters were available, the crater-floor mounds are identified as discrete

138   rises from the crater floor, noted by a distinct break in slope. In the absence of topographic data

139   the shadows cast by the mounds are relied on for identification; thus, the estimate for these

140   craters is conservative. Mound-distribution density is calculated by means of four steps. 1.

141   identifying the location of the mound(s) furthest from the crater-floor centre; 2. measuring the

142   radius between the two points; 3. using this radial distance and, derivatively, circumference to

143   calculate floor-surface area (km^2); and, 4. dividing the surface area by the number of mounds

144   located therein. Mound heights for two of the studied craters are measured using elevation data

145   derived   from   HiRISE   stereo-pairs   (ESP_017525_2475,   ESP_017090_2475   and

146   ESP_018210_2445, ESP_018078_2445) using the methods described by Kirk et al. (2008) at the

147   NASA RPIF3D facility at UCL. Using the method of Okubo (2010), we estimate the vertical

148   precision of these two DEMs to be 0.23m and 0.18m respectively. Only mounds that are not

149   clustered tightly with others are used for height measurements so as to obtain a reliable base-

150   height. Heights are taken as the difference between highest and lowest elevation value within the

151   polygon delimiting the mound. Our discussion integrates the spatial location of craters

152   containing paleo-lakes as presented in Table 1 of El Maarry et al. (2010). The set of craters

153   analyzed in this investigation is a subset of the population discussed in their recent study.

154   ***3. Mound morphology, traits and spatially associated crater-floor features in northern Utopia***

155   ***Planitia***

156   Pingo-like mounds are ubiquitous on Mars, albeit mainly at mid or equatorial latitudes

157   (Dundas et al., 2010), and have been discussed by a multiplicity of workers: i.e. Acidalia Planitia

158   (Lucchitta, 1981); the Athabasca Valles and the Cerberus Plains (Burr et al., 2005; Page and

159   Murray, 2006; Page, 2007; Balme and Gallagher, 2009), Maja Valles (Theilig and Greeley,

160   1979); and mid Utopia Planitia (Dundas et al., 2008; Burr et al., 2009; de Pablo and Komatsu,

161   2009; Lefort et al., 2009; Dundas and McEwen, 2010). By contrast, the putative CSPs observed

162   by us occur uniquely at near-polar latitudes in the northern hemisphere (64-69°N) **(Fig. 3)**.

163   Through the past few years Bruno et al. (2006), Dundas et al. (2008, 2010) and Burr et al.

164   (2009a, b) have urged caution in the reporting of pingo-like mounds and suggested that much

165   work remains before pingo hypotheses are validated. In particular, Dundas et al. (2010) points to

166   the apparent contradiction between a late-Amazonian Epoch that is thought to be highly arid and

167   the water volume requirements of pingo hypotheses. We address some of their concerns below

168   (cf. section 4.3.2).

169   In our study region (a circum-global transect comprising   55-70°N), the floors or basins

170   of five impact-craters show spatially-associated complexes of small-sized unsorted polygons and

171   mounds whose size, shape, key geological characteristics and distribution are consistent with

172   thermokarst-lake or alas/CSP assemblages such as those located in the TC (**Fig. 3**). Table 1

173   presents the images used for each of these craters in the following analyses.

174   Host crater-diameters range from   7-19km (**Table 2**) and none of their ejecta deposits

175   exhibit inward-oriented breaches or flow features. Sixty-seven other craters at or above the

176   minimum crater diameter of   7km were imaged by the MOC and HiRISE cameras but did not

177   show spatially-associated complexes of polygons and mounds. Host crater-depths are shallow

178   compared with global crater depth-diameter estimates (Garvin et al., 2003)(**Fig. 4**, **Table 2**).

179   However, this is consistent with the measurements of crater depths in the   10-25km diameter

180   range above 52°N made by Kreslavsky and Head (2006). Intriguingly, each of the polygon and

181   mound-bearing craters occur in northern UP within a tight latitudinal band (~64-69°N) and a

182   narrow longitudinal reach (~26-98°E). This could be indicative of surface and/or atmospheric

183   boundary conditions that are highly localised and possibly consistent with landscape

184   modification by periglacial processes.

185   Mound diameters range from tens to hundreds of metres (**Figs. 5 and 6, Table 2**); mound

186   heights extend from ~6-33m (**Table 2, Fig. 5**). In cross-section, the mounds are conical to

187   domical in shape and have low flank-slopes of up to ~15° (**Fig. 5**). We do not observe summit

188   fractures as seen in many pingos in TC but occasionally circular raised-rims with basal diameters

189   similar to those of the crater-floor mounds are observed in proximity to these mounds (**Fig. 6**).

190   These could be mound remnants or slump markers. Mound shape in plan view is circular to

191   elongate (**Figs. 5 and 6**); mound distribution is clustered around or at the crater-floor centres.

192   Mound density in **Fig. 5** is ~0.9 mounds/km^2 and 0.4 mounds/km^2 in **Fig. 6** (also, cf.

193   supplementary **Figure 1).** Some mounds are nested directly on the crater floor; others, seem to

194   lie atop ridge-like structures that show a ring-like appearance **(Fig. 6)**.

195   All of the mound-bearing craters display floors dominated by unsorted polygonal-

196   patterned ground ≤~350m in diameter **(Fig. 6)**. Polygonisation is typical of the terrain within and

197   around impact craters at this latitude (Gallagher et al., 2011). Some of crater-floor polygons

198   cross-cut the mounds (**Fig. 5C**); others show an orthogonal orientation **(Fig. 6)**. Recent estimates

199   of crater-retention ages at this latitude, using the Heimdal Crater (68.3°N; 235.2°E) as a

200   benchmark, suggest that the polygonised terrain is within the   0.5-2.0 Ma range (Gallagher et

201   al., 2011).

202   *4. Discussion - Mound Origins*

203   Here we consider three mound-formation hypotheses in the light of our new observations

204   as well as the recent work of Conway et al. (2012) and El Maarry et al. (2010, 2012).

205   *4.1   Weathered uplift-complexes*

206   On Mars, small (< 5km) impact craters are noted for having a relatively simple, bowl-

207   shaped geometry (Werner et al., 2004; Wood et al., 1978). Large craters, particularly those above

208   the ~8-10km range of diameter, exhibit complex morphologies that include terraced walls and

209   regions of central uplift (Garvin et al., 2003; Wood and Andersson, 1978). Central uplift occurs

210   in the modification and collapse phase of crater formation, following the formation of a transient

211   cavity, as weak material collapses and returns to a state of gravitational equilibrium (Bond, 1981;

212   Melosh, 1989). Regions of central uplift are typically domical, have one or several peaks, and

213   exhibit maximum heights that are well below crater-rim crests and the level of surrounding

214   plains (Bond, 1981).

215   There are two general observations suggesting that the observed mounds are weathered

216   and/or partially-buried remnants of central-uplift material: 1. the mounds are clustered in the

217   central region of the crater floors; and, 2. the craters in which they lie are above the threshold

218   diameter for central-uplift formation. Under this scenario the central-uplift structures or

219   complexes would have gradually undergone burial by sedimentation; once the crater-fill was

220   sufficiently thick only the uplift summits would be visible, somewhat like nunataks in the

221   Antarctic (**Fig. 7**). Weathering and erosion could have carved these structures into mounds

222   similar in appearance to the ones observed on the crater-floors of UP. This scenario is consistent

223   with the fact that craters serve as traps for dust and regolith over time and that our studied craters

224   are observed to have relatively shallow depths (**Fig. 4**). Some authors have suggested that high-

225   northern craters might be filled with dusty-ice (e.g. Kreslavsky and Head, 2006) and/or

226   sediments deposited during the presence of a northern ocean (e.g. Boyce et al., 2005).

227   The plausibility of the central-uplift hypothesis is contingent upon crater-fill levels lying

228   below the upper elevation-threshold of impact-related crater-floor structures. Even though

229   accurate *in situ* measurements of fill depths are not available, estimates of fill depth can be

230   calculated by using 1. MOLA profiles to identify crater diameters and rim elevations; and, 2.

231   generally-accepted assumptions concerning the depth-to-diameter dimensions of complex

232   craters. The latter comprise the following:

233   (a) Crater diameter is stable over time, changing by no more than 10-15% from its initial

234   value as craters degrade (Craddock and Maxwell, 1990).

235   (b) Crater depth is diameter dependent and relatively accurate predictions of initial crater

236   depth can be made from generalized formulae (Boyce et al., 2005; Garvin et al., 2003;

237   Stewart and Valiant 2006).

238   (c) The height of central-uplift structures is diameter dependent and is well below the

239   level of the surrounding plains (Garvin et al., 2003; Werner et al., 2004).

240   Using these assumptions we have identified five key characteristics of the five principal

241   mound-bearing craters and summarise them here; more detail is available in Table 2: 1. rim-to-

242   floor/top of fill depth (actual); 2. initial depth (estimated); 3. initial depth (estimated) to current

243   floor (actual); 4. central-peak height (estimated); and, 5. height difference (estimated) between

244   the current floor (actual) and the central-peak summit (estimated). Each of the mound-bearing

245   craters show a minimum height difference of ~600m between the fill/crater floor level and the

246   buried summit of the crater's central peak **(Table 2)**. This difference of height is exemplified by

247   comparing a MOLA profile that crosses the crater floor and central peak of a non mound-bearing

248   complex crater in the northern plains (**Fig. 8a**) with a MOLA profile that crosses one of the five

249   mound-bearing craters in the region (**Fig. 8b**).

250   As the crater-floor mounds and spatially-associated ridges occur well above the heights

251   predicted for central peaks in each of the mound-bearing craters, this suggests that the mounds

252   and ridges could not be partially-exposed central peaks or peak remnants. Interestingly, Stewart

253   and Valiant (2006) suggest that Garvin's formulae underestimate the initial depth of complex

254   impact-craters in some areas of the northern plains.

255   Are the initial depths of impact craters in the high northern plains shallower than

256   elsewhere on Mars? Based on the following observations this seems unlikely: 1. the

257   morphological traits associated with the high-northern craters, such as ejecta smoothing, are

258   consistent with them having experienced high levels of infilling and modification (Garvin et al.,

259   2003; Kreslavsky and Head, 2006); 2. there are some relatively pristine craters (distinguished by

260   rough and easily visible ejecta-blankets) in this region that have depths exceeding the predicted

261 initial depth for craters with specific diameters derived of global averages (Garvin et al.,

262 2003)(**Fig. 4**); and, 3. although variation in the lithology of impact targets has an influence on

263 initial crater geometry (e.g., as summarized in Stewart and Valiant, 2006), significant infilling is

264 still implied by the shallow depths observed in the mound-bearing craters compared to other

265 craters in the surrounding area (**Fig. 4**).

266 Finally, if we consider that the craters in our study are outliers to the general population

267 and therefore anomalously shallow then does the small-scale morphology of the mounds make

268 sense as central complex remnants? Without a concrete example of a deeply buried central-uplift

269 elsewhere on Mars we cannot compare directly the dimensions and density of mounds that we

270 observe in UP. However, for craters 2 and 5 in particular it seems unlikely that a central-uplift

271 complex could possess so many and such widely distributed (from the crater centre to within

272 ~2km of the crater rim) peaks of almost the same height.

273 In summary, it is unlikely that these mounds are remnants of central uplift complexes,

274 because the implied level of fill surpasses estimated uplift-elevations by over 600m (**Table 2**);

275 moreover, in some cases the mound morphology is not consistent with the expected morphology

276 of buried central-uplift complexes.

277 *4.2 Impact-related hydrothermal structures*

278 Impact-related hydrothermal activity (Newsom, 1980) could be the progenitor of the

279 crater-floor mounds. For example, amongst the geological traits observed at the Hesperian-aged

280 Toro impact crater on the northern edge of the Syrtis Major Volcanic Plains (17.0°E; 289.2°N)

281 are mounds, polygonal fractures, veins and structural discontinuities that could be the result of

282 volatile release and/or liquid flows (Fairen et al., 2010; Marzo et al., 2010). Distinctive

283 mineralogy and abundances of hydrated phases in and around the central-uplift complex, perhaps

284 associated with impact-melt bearing crater-fill deposits, also are consistent with a hydrothermal

285 origin of these structures (Marzo et al., 2010). The mounds and polygonal cracks observed here

286 have similar dimensions to those that we observe in UP **(Fig. 9);** however, the close spatial-

287 association of the mounds and polygons is not observed.

288   By a similar argument to that which is made for the central-uplift remnant hypothesis, the

289 hydrothermal hypothesis can also be rejected. Although some of the crater fill in the mound-

290 bearing craters could be associated with the impact formation of the craters themselves, the fill

291 height of these craters exceeds the hypothesised level of impact-related melt material as well as

292 central peak summits. For example, Toro crater is ~40km in diameter, has a rim to floor depth of

293 ~2km and the central-peak summit rises   400m above the current crater floor (Marzo et al.,

294 2010). By fitting a planar surface through the MOLA data exterior to this crater's ejecta; we

295 were able to estimate the elevation difference between the plains and the central peak as ~960m.

296 This means that the elevation of the central-uplift structure and, derivatively, the impact-related

297 fill deposits, lie well below the elevation datum of the surrounding plains. In addition, although

298 the mounds in Toro are located near the centre of the crater they are not atop the central uplift;

299 this is where you would expect them to be located if they were exposed sub-aerially subsequent

300 to the infilling of the host crater. By contrast, the putative CSPs in northern UP lie atop hundreds

301 of metres of fill, almost at the elevation datum of the surrounding plains (Soare et al., 2011b).

302 *4.3 Perennial ice-cored mounds (pingos)*

303   *4.3.1 Thermokarst lakes on Earth and the possible origin of closed-system pingos*

304   In periglacial landscapes such as the TC, closed-system pingos form where thermokarst

305 lakes either have lost or are in the process of losing their water by drainage or evaporation

306 (Mackay, 1998) **(Fig. 1)**. Exposure of the previously unfrozen lake-floor to freezing temperatures

307 leads to permafrost aggradation downwardly through the lake-floor sediments and inwardly from

308 the lake margin (Mackay, 1998). As the permafrost aggrades, pore water is placed under

309 increasing hydrostatic pressure and migrates away from the freezing fronts. Impelled by this

310 pressure, the pore water uplifts and deforms the newly frozen lake-floor; this happens at or near

311 the centre of the lake-floor where the permafrost is particularly thin and where small residual

312 ponds may occur (Mackay, 1998). When the pore water (injection ice) freezes beneath the

313 uplifted lake floor an ice-core forms, providing the buttress of a perennial sediment-covered

314 mound or pingo (Washburn, 1973, Mackay, 1998; French, 2007)

315   Polygonal-patterned ground formed by thermal-contraction cracking often surrounds and

316 cross-cuts the pingos **(Fig. 2b)**; ice wedges, the product of seasonal thaw, underlie polygon

317 margins or troughs. In some instances, the polygons may show an orthogonal orientation (Soare

318 et al., 2008, 2011a); this is a marker of the episodic loss of water in a thermokarst lake

319 (Lachenbruch, 1962). When their ice-cores degrade and the mounds undergo ablation, slump

320 material forms a raised-rim mound remnant **(Fig. 2c)** (Mackay, 1998; Washburn, 1973).

321   The Martian crater-floor mounds approximate terrestrial CSPs (of the TC type) in shape,

322 size and spatial association with small-sized polygonal patterned-ground. In a survey of 1247

323 pingos (of which 98% are estimated to be hydrostatic) in Arctic Coastal Plain, northern Alaska,

324 Jones et al. (2012) find that pingo heights range from 2 to 21m (mean 4.6m), diameter 32 to

325 295m (mean 94m) and maximum density of 0.18 per km^2. A similar study of 3109 mostly

326 hydrostatic pingos in northern Asia (Grosse and Jones, 2011) found that pingo heights range

327 from 2-37m (mean 4.8m), and have a maximum density of 0.28 per km^2. Hence, the UP

328 mounds are slightly larger on average compared to pingo populations on Earth but they do have a

329 similar height-to-diameter ratio. The density of the UP pingos is slightly higher than that

330 reported in the Jones et al. (2012) and Grosse and Jones (2011) studies; however if we consider a

331 single basin in TC, we obtain a density of 3 per km^2, hence the measurement of the density of

332 pingos is susceptible to the scale considered. Pingos undergoing degradation on Earth often

333 possess summit cracks, but we do not observe this in UP. The absence of summit cracks on the

334 mounds in UP does not rule them out as being pingos, as many pingos on Earth never reach the

335 threshold of size and stress for this to occur.

336   Of the three hypotheses presented and discussed above, the periglacial or closed-pingo

337 system hypothesis also is the only one that is stratigraphically consistent with the depth

338 calculations (initial and actual) of the mound-bearing complex craters in northern UP. That is to

339 say, if the pingo-like mounds comprise post-fill structures or structures associated with a post-fill

340 revision of the near-surface regolith, then their occurrence atop the fill would be expected.

341 *4.3.2 Late Amazonian crater-lakes and climatic water-ice accumulation*

342   In their recent work Conway et al. (2012) have documented eighteen (km-scale) impact

343 craters at latitudes ≥70°N that host large (mostly km-scale) perennial domes. Spectral data

344 acquired by the MEX OMEGA (Mars Express, Observatoire pour la Minéralogie, l'Eau, les

345 Glaces et l'Activité) show high water-ice concentrations (up to 0.7 band depth) at the surface of

346 some of these (Conway et al., 2012). None of the host craters are smaller than 9.5 km in

347 diameter; ten craters exhibit diameters from 9.5-20km. The maximum thickness of their water-

348 ice domes ranges from 94-1640m and the ice mound-summit-to-rim distance varies from 13-

349 626m. Interestingly, each of the impact craters that show pingo-like mounds on their floors have

350 diameters between 7.3-18.8 km (cf. Table 2).

351   Conway et al. (2012) hypothesise that these massive ice-domes form from water-ice

352 vapour transported from the north-polar region and cold-trapped in their host craters **(Fig. 10)**.

353 Cold-trapping could be triggered by the higher atmospheric pressure and lower temperature of

354 crater interiors; in turn, this would increase the accumulation rates of water-ice during the winter.

355 Were accumulation significant enough then this water-ice could be preserved through the spring

356 and summer when the seasonal polar cap retreats, creating a perennial ice-dome. Once formed,

357 the ice domes comprise a positive feedback-loop whereby their high albedo and high thermal-

358 inertia but low temperatures are a permanent cold trap for condensation.

359   Similar domes could have evolved in the craters where the putative CSPs occur, under

360 orbital parameters where the stability zone of ice-dome formation extends slightly further to the

361 south than is the case currently (64°N, according to the southern-most crater where the CSPs

362 are located). This is likely to be a period with higher obliquity and/or eccentricity that lengthens

363 the northern-winter. When Mars returns to antecedent orbital-parameters the stability zone of

364 ice-dome formation in the northern hemisphere would migrate polewardly; depending upon

365 regional boundary conditions the more southerly domes either would sublimate or thaw, pool and

366 form endogenic paleo-lakes.

367   Indirect evidence of paleo-lakes having formed at the latitudes of the current ice-domes

368 and the putative CSPs has been reported by El Maarry et al. (2008, 2010). They have studied the

369 fracture mechanics of crater-floor polygons at near-polar latitudes in the northern hemisphere of

370 Mars. The polygons range in diameter from ~15-350m and are located principally between 65-

371 75°N (El Maarry et al., 2010)(**Fig. 3**). El Maarry et al. (2010) hypothesise that under present

372 boundary conditions the crater-floor polygons with diameters $\geq$ 75m can be formed only by

373 desiccation, not by sublimation-related processes; if so, then this points to the antecedent

374 occurrence of paleolakes in the host crater-basins (El Maarry et al., 2010). With regard to the

375 crater-floor polygons $\leq$75 m, their formation could be the result of desiccation (El Maarry et al.,

376 2010) or thermal contraction (El Maarry et al., 2010; also, Soare et al., 2005). Polygon formation

377 by means of thermal-contraction cracking, particularly when the polygons exhibit an orthogonal

378 orientation as some of them do in the putative CSP craters, also points to periglacial processes at

379 work in a lacustrine environment (Lachenbruch, 1962).

380 Two other landscape characteristics are consistent with the antecedent occurrence of

381 paleolakes in the CSP impact craters: ridge-like structures on the crater floors and the relative

382 location of the CSPs themselves. With regard to the former, these might be sedimentary markers

383 or paleo-shorelines of a lake in recession or of residual ponds forming prior to the complete loss

384 of lake water on the crater floor. On the other hand these ridges could be indicative of a

385 structural control on the migration of subsurface volatiles, as there is often a genetic/spatial

386 linkage among tectonic (e.g., faults and joints), and emplaced (e.g., dikes and elongated plugs,

387 hydrothermal mounds, migrating pingos) landforms (Dohm, 1995, Dohm et al., 2001; Tanaka et

388 al., 1998; Wu et al., 2005).

389 With regard to the latter, and as noted above, the formation of CSPs on Earth tends to

390 occur at or near the centre of a host thermokarst lake, this being the site of thin permafrost where

391 remnant water pools last (Mackay, 1998). The putative Martian CSPs show clustering at or near

392 the centre of their host craters that is consistent with terrestrial thermokarst-lake/CSPs

393 assemblages (Fig. 1g).

394 A possible constraint on the CSP hypothesis concerns the availability of liquid water

395 volumetrically sufficient to generate CSPs on crater floors at high northern latitudes (Dundas et

396 al., 2010). However, the current thicknesses and summit-to-rim distances of ice domes in craters

397 comparable in diameter to those hosting pingo-like mounds suggest that the water requirements

398 of the latter can be met were pre-cursor ice-domes to have formed in the mound-bearing craters.

399 As noted above, ice dome thicknesses in craters with diameters of 9.5-20km ranges from tens to

400 hundreds of metres and summit-to-rim distances comprise hundreds to thousands of metres in

401 reach (Conway et al., 2012).

402   Using a DEM we have calculated the heights of two putative CSPs (15m, cf. Table 2).

403 Even if one assumes a volumetric loss of 9% when water ice changes phase to liquid water as an

404 ice domes thaws and melt-water pools on a crater floor, ice-dome thickness largely exceeds the

405 height of the pingo-like mounds by an order of magnitude. In some instances, summit-to-rim

406 distances also exceed mound diameters by an order of magnitude.

407 *Conclusion*

408   Compared to the alternative hypotheses, the periglacial hypothesis is much more robust

409 and coherent in explaining crater-floor mound formation in northern UP. It integrates

410 geomorphological, stratigraphical and climatological observations, assumptions and estimates

411 whereas the alternatives do not. Moreover, only the periglacial hypothesis is consistent with fill-

412 depth estimates of the mound-bearing impact craters.

413   In terms of shape, size key geological characteristics and distribution, the crater-floor

414 mounds of northern UP are consistent with the shape, size, key geological characteristics and

415 distribution of CSPs in terrestrial periglacial-environments such as the Tuktoyaktuk Coastlands.

416 Moreover, regardless of whether the small-sized polygons located in craters with pingo-like

417 mounds are the result of desiccation or thermal contraction, both processes are associated with

418 lake evolution on Earth and are consistent with the CSP hypothesis.

419   We suggest that the landscape assemblage comprised of crater-floor pingo-like mounds

420 and small-sized polygons is a paleo-marker of freeze-thaw cycling and of a surface /near-surface

421 system, albeit a highly localised one, rich in water. Consequently, the atmospheric boundary

422   conditions of temperature, atmospheric pressure and humidity required to initiate and maintain

423   the freeze-thaw cycling of water would have been much higher than many workers have thought

424   possible in the region during the late Amazonian Epoch.

431   **References**

432   Balme, M.R., Gallagher, C., 2009. An equatorial periglacial landscape on Mars. *Earth and*

433   *Planetary Science Letters* 285 (1-2) 1-15, doi:10.1016/j.epsl.2009.05.031.

434   Bond, J. W., 1981. The development of central peaks in lunar craters, *The Moon, and the Planets*

435   25, 465-476.

436   Boyce, J.M., Mouginis-Mark, P., Garbeil,, H. 2005. Ancient oceans in the northern lowlands of

437   Mars: Evidence from impact crater depth/diameter relationships. *Journal of Geophysical*

438   *Research*, 110 (E3) doi:10.1029/2004JE002328.

439   Bruno, B.C., Fagents, S.A., Hamilton, C.W.,Burr, D.M., Baloga, S.M., 2006. Identification of

440   volcanic rootless cones, ice mounds, and impact crater on Earth and Mars: Using spatial

441   distribution as a remote sensing tool. Journal of Geophysical Research 111, E06017,

442   doi:10.1029/2005JE002510.

443   Burr, D.M., Soare, R.J., Wan Bun Tseung, Emery, J.P., 2005. Young (late Amazonian) near-

444   surface ground-ice features near the equator. *Icarus* 178 (1) 56-73, doi:10.1016/2005.04.

445   012.

446   Burr, D.M., Bruno, B.C., Lanagan, P.D., Glaze, L.S., Jaeger, W.L., Soare, R.J., Wan Bun

447   Tseung, J.M., Skinner, J.A., Baloga, S.M., 2009a. Mesoscale raised rim depressions

448   (MRRDs) on earth: A review of the characteristics, processes, and spatial distribution of

449   analogs for Mars. Planetary and Space Science 57, 5-6, 579-596,

450   doi.org/10.1016/j.pss.2008.11.011.

451   Burr, D.M., Tanaka, K.L., Yoshikawa, K., 2009b. Pingos on Earth and Mars. *Planetary and*

452   *Space Science* 57, 5-6, 541-555. doi.org/10.1016/j.pss.2008.11.003.

453   Conway, S.J., Hovius, N., Barnie, T., Besserer, J., Le Mouélic, S., Orosei, R., Read, N.A., 2012.

454   Climate-driven deposition of water ice and the formation of mounds in craters in Mars'

455   North Polar region. *Icarus* 220, 1, 174-193, dx.doi.org/10.1016/j.icarus.2012.04.021

456   Craddock., R.A., Maxwell. T.A., 1990. Resurfacing of the Martian highlands in the Amenthes

457   and Tyrrhena Region. *Journal of Geophysical Research* 95 (B9) 14,265-14,278.

458   de Pablo, M.A., Komatsu, G., 2009. Possible pingo fields in the Utopia basin, Mars: Geological

459   and climatical implications. *Icarus* 199 (1) 49-74, doi:10.1016/j.icarus.2008.09.007.

460   Dohm, J.M., 1995. Origin of Stoneman lake, and volcano-tectonic relations of Mormon

461   and San Francisco volcanic fields, Arizona, M.S. thesis, Northern Arizona

462   University, Flagstaff, Arizona, 101 p.

463   Dohm, J.M., Tanaka, K.L., Hare, T.M., 2001. Geologic map of the Thaumasia region of Mars.

464   *USGS Misc. Inv. Ser*. Map I-2650, scale 1:5,000,000.

465   Dundas, C.M., Mellon, M.T., McEwen, A.S., Lefort, A., Keszthelyi, L.P., Thomas, N., 2008.

466　　　　HiRISE observations of fractured mounds: Possible Martian pingos. *Geophysical*

467　　　　*Research Letters* 35, L04201, doi:10.1029/2007GL031798.

468　Dundas, C.M., McEwen, A.S., 2010. An assessment of evidence for pingos on Mars using

469　　　　HiRISE. Icarus 205, 244-258, doi:10.1016/j.icarus.2009.02.020.

470　El Maarry, M.R., Markiewicz, W.J., Mellon, M.T., Goetz, W., Dohm, J.M., Pack, A., 2010.

471　　　　Crater Floor Polygons: Desiccation Patterns of Ancient Lakes on Mars? *Journal of*

472　　　　*Geophysical Research* 115 (E10006) doi:10.1029/2010JE003609.

473　Fairén, A.G. et al., 2010. *Proceedings of the National Academy of Sciences* 107, 12,095-12,100,

474　　　　doi:10.1073/pnas.1002889107.

475　French, H.M., 2007. *The periglacial environment*, 3rd edition. Wiley, West Sussex, England,

476　　　　458 p.

477　Gallagher, C., Balme, M.R., Conway, S.J., Grindrod, P.M., 2011. Sorted clasted stripes, lobes

478　　　　and associated gullies in high latitude craters on Mars: landforms indicative of very

479　　　　recent polycyclic ground-ice thaw and liquid flows. *Icarus* 211, 458-471. doi:10.1016/

480　　　　j.icarus.2010.09.010.

481　Garvin, J.B., Sakimoto, S.E.H., Frawley, J.J., 2003. Craters on mars: global geometric

482　　　　properties from MOLA gridded topography. *6th Mars Conf.* Abstract # 3277.

483　Grosse, G., Jones, B.M., 2011. Spatial distribution of pingos in northern Asia. *The Cryosphere* 5,

484　　　　13-33, doi:10.5194/tc-5-13.

485　Hamilton, T.D., Obi, C.M., 1982. Pingos in the Brooks Range, northern Alaska, USA. *Arctic and*

486　　　　*Alpine Research* 14 (1) 13-20.

487　Harris, S.A. et al., 1988. Glossary of permafrost and related permafrost terms. Permafrost

488   Subcommittee, Associated Committee on Geotechnical Research, National Research

489   Council of Canada, Ottawa, Technical Memorandum 142, 156 p.

490 Hauber, E., Reiss, Ulrich, M., Preusker, F., Trauthan, F., Zanetti, M., Hiesinger, H., Jaumann, R.,

491   Johansson, L., Johnsson. A., Van Gasselt, S., Olvmo, M., 2011. Landscape evolution in

492   Martian mid-latitude regions: insights from analogous periglacial landforms in Svalbard.

493   *Geological Society, London, Special Publications,* 356, 111-131, doi:10.1144/SP356.7.

494 Jones, B M., Grosse, G., Hinkel, K.M., Arp, C.D., Walker, S., Beck, R.A., Galloway, J.P., 2012.

495   Assessment of pingo distribution and morphometry using an IfSAR derived digital

496   surface model, western Arctic Coastal Plain, Northern Alaska. *Geomorphology* 138 (1) 1-

497   14. doi:10.1016/j.geomorph.2011.08.007.

498 Kirk, R.L., Howington-Kraus, E., Rosiek, M.R., Anderson, J.A. , Archinal, B.A., Becker, K.J.,

499   Cook, D.A. et al., 2008. Ultrahigh resolution topographic mapping of Mars with MRO

500   HiRISE stereo images: Meter-scale slopes of candidate Phoenix landing sites. *Journal of*

501   *Geophysical Research (Planets)* 113, doi:10.1029/2007JE003000.

502 Kreslavksy, M.A., Head, J.W., 2006. Modification of impact craters in the northern plains of

503   Mars. Implications for Amazonian climate history. *Meteoritics and Planetary Science* 41

504   (10) 1633-1646.

505 Lachenbruch, A.H., 1962. *GSA Special Paper 70.* New York: Geological Society of America, 69

506   p.

507 Lefort, A., Russell, P.W., McEwen, A.S., Dundas, C.M., Kirk, R.L., 2009. Observations of

508   periglacial landforms in Utopia Planitia with the High Resolution Imaging Science

509   Experiment (HiRISE). *Journal of Geophysical Research* 114 (E04005) doi:10.1029/

510   2008JE003264.

511   Lucchitta, B., 1981. Mars and Earth: comparison of cold-climate features. *Icarus* 45, 264-303.

512   Mackay, J.R., 1998. Pingo growth and collapse, Tuktoyaktuk peninsula area., western Arctic

513   coast, Canada: a long-term study. *Géographie physique et Quaternaire* 52 (3) 1-53.

514   Marzo, G.A. et al., 2010. Evidence for Hesperian impact-induced hydrothermalism on Mars.

515   *Icarus* 208 (2) 667-683, doi:j.icarus.2010.03.013.

516   Melosh, H.J., 1989. Impact cratering: a geologic process: New York, Oxford University Press,

517   245 p.

518   Newsom, H.E., 1980. Hydrothermal alteration of impact melt-sheets with implications for

519   Mars. *Icarus* 44, (1) 207-216.

520   Okubo, C.H., 2010. Structural geology of Amazonian-aged layered sedimentary

521   deposits in southwest Candor Chasma, Mars. *Icarus* 207, 210-225, doi:10.1016/j.icarus.

522   2009.11.012.

523   Page, D.P., 2007. Recent low-latitude freeze-thaw on Mars. *Icarus* 189 (1) 83-117, doi:10.1016/

524   j.icarus.2007.01.005.

525   Page, D.P., Murray, J.B., 2006. Stratigraphical and morphological evidence for pingos in the

526   Cerberus plains. *Icarus* 183 (1) 46-54, doi:10.1016/j.icarus.006.01.017.

527   Soare, R.J., Burr, D.M., Wan-Bun Tsueng, J.M., 2005a. Possible pingos and a periglacial

528   landscape in Utopia Planitia, Mars. *Icarus* 174 (2) 373-382, doi:10.1016/j.icarus.2004.

529   11.013.

530   Soare, R.J., Burr, D.M., Wan-Bun Tseung, J.M., Peloquin, C., 2005b. Possible pingos and

531   periglacial landscapes in northwest Utopia Planitia. *LPS XXXVI*, Abstract # 1102.

532   Soare, R.J., Osinski, G.R., Roehm, C.L., 2008. Thermokarst lakes and ponds on Mars in the

533   very recent (late Amazonian) past. *Earth and Planetary Science Letters* 272 (1-2) 382-
534   393, doi:10.1016/j.epsl.2008.05.010.

535 Soare, R.J., Séjourné, A., Pearce, G., Costard, F., Osinski, G.R., 2011a. The Tuktoyaktuk
536   Coastlands of northern Canada: a possible "wet" periglacial analogue of Utopia Planitia,
537   Mars. *Geological Society of America Special Paper* 483, doi:10.1130/2011.2483(13).

538 Soare, R.J., Costard, F., Pearce, G., 2011b. Possible pingos and crater-floor periglacial
539   landscapes in northwest Utopia Planitia: a re-assessed hypothesis based on Hi-RISE
540   imagery. *LPS XXXXII*, Abstract # 1364.

541 Stewart, S.T., Valiant, G.J., 2006. Martian subsurface properties and crater formation processes
542   inferred from fresh impact crater geometries. *Meteoritics and Planetary Science* 41 (10)
543   1509-1537, doi:10.1111/j.1945-5400.2006.tb00433.x

544 Tanaka, K.L., Dohm, J.M., Lias, J.H., Hare, T.M., 1998. Erosional valleys in the Thaumasia
545   region of Mars: hydrothermal and seismic origins. *Journal of Geophysical Review* 103,
546   31,407-31,419 doi:10.1029/98JEO1599.

547 Theilig, E., Greeley, R., 1979. Plains and channels in the Lunae Planum-Chryse Planitia
548   Region of Mars. *Journal of Geophysical Research* 84 (B14) 7994-8010.

549 Washburn, A.L., 1973. *Periglacial processes and environments*. St. Martin's Press, New York,
550   N.Y.

551 Werner, S.C., Ivanov, B.A., Neukum, G., 2004. Impact cratering on Mars: Search for target
552   influence on morphology. *LPS XXXV*, Abstract #1953.

553 Wood, C.A., Head, J.W., Cintala, M.J., 1978. Interior morphology of fresh Martian craters-The
554   effects of target characteristics. *LPS IX*, pp. 3691-3709.

555 Wu, Z. et al., 2005. Migrating pingos in the permafrost region of the Tibetan Plateau, China and

556   their hazard along the Golmud-Llasa railway. *Engineering Geology* 79 (3-4) doi:10.1016/

557   jenggeo.2005.02.003.

558 **Figures**

559 **1.** The Pingo Canadian Landmark is a national park 6km southwest of Tuktoyaktuk adjacent

560   to the Beaufort Sea in the Tuktoyaktuk Coastlands of northern Canada. Image (A27917-35-

561   1993) courtesy of the Canadian Air Photo Library. Amongst the numerous pingos located

562   here are Ibyuk (circular and ~49m in height) at the right; Split (sub-circular and ~ 35m in

563   height) at the centre; and, an un-named elongated pingo at the top of the image on the left.

564 **2. a-e)** An idealised schema of closed-system pingo evolution in the Tuktoyaktuk Coastlands

565   (TC) of northern Canada (Mackay, 1998). This is discussed in detail in Section 4.3.1. **f)** A

566   small thermokarst lake surrounded by thermal-contraction polygons (TC, early July 2007).

567   Image credit: R. Soare. **g)** A three-pingo complex in the midst of a thermokarst lake losing its

568   water by evaporation and/or drainage. Note the un-vegetated and pale margins of the lake

569   and pingos, indicative of water loss that is relatively recent (TC, early July 2007). Image

570   credit: R. Soare. **h)** The end-stage of pingo evolution is a raised-rim landform or scar

571   comprised of slump material, as exemplified by this oblique view of a collapsed pingo in the

572   Brooks Mountains of Alaska (Hamilton and Obi, 1982).

573 **3.** Map showing the spatial distribution of mound-bearing impact craters in northern Utopia

574   Planitia: the map incorporates a MOLA hillshade-background image (courtesy of

575   www.jpl.nasa.gov) and the following CTX images comprise the crater mosaic below the

576   map: B02_010392_2491, P16_007372_2474, B22_018078_2445, P19_008492_2446,

577   B19_017089_2341 and B19_017154_2472 (courtesy of MSSS/Caltech/JPL).

578 **4.** Depth-diameter plot of the craters in the region local to those containing mounds, i.e. 62-

579   70°N and 26-98°E, as mapped by Conway et al. (2012). The craters with mounds and the

580   craters mapped as containing evidence of crater lakes by El Maarry, et al. (2010) are

581   highlighted. The depth-diameter relationship found by Garvin et al. (2003) is included as a

582   reference.

583 **5.** Mounds on the floor of crater # 2, HiRISE image ESP_017090_2475 (courtesy of

584   NASA/JPL/U of A) overlain on CTX image P16_007372_2474 (courtesy of

585   MSSS/Caltech/JPL). 10m contours are derived from a 1m/pixel DEM produced from HiRISE

586   images ESP_017525_2475, ESP_017090_2475. Online version has a color-drape which was

587   derived from the HiRISE DEM. Stars indicate the locations of the mapped mounds used to

588   produce the statistics in Table 2. Cross-sections whose locations are indicted on the image

589   insets A-C are also derived from the same elevation data.

590 **6.** Mounds in crater # 3, HiRISE image PSP_007780_2450; 64.5°N, 63.7°E; 25 cm/pixel

591   (courtesy of NASA/JPL/U of A). Note the diversity of mound morphology, highlighted in the

592   white boxes: i) circular, ii) elongate and iii) remnant, possibly a mound scar. Clustering at or

593   near the crater-floor centre is a keynote of mound distribution, as is a ring-like appearance.

594 **7.** Central peak of well-preserved crater northwest of Tartarus Montes: HiRISE

595   PSP_009240_2055; 25.0°N, 167.6°E; 25 cm/pixel (courtesy of NASA/JPL/U of A).

596 **8.** **a)** Plan and profile view of a ~13.5km diameter mound-bearing crater at 67.2°N, 47.8°E. The

597   solid black line is derived from MOLA profile 20037 and presents the level of the crater floor

598   to be very near that of the surrounding plains. The serrated black line shows an estimate for

599   the initial depth of the crater based on a power law derived from Garvin et al. (2003). CTX

600   image P16_007372_2474 was used for the top of the figure (courtesy of CalTech/JPL). **b)**

601   Plan and profile view of a ~18.7km diameter crater with a central peak at 38.6°N, 137.2°E.

602   MOLA profile 12352 crosses the crater's central peak, indicating that it is well below the

603   level of the surrounding plains. Crater image is cropped from THEMIS visible wavelength

604   image V09919018 (courtesy of NASA/JPL/ASU).

605 **9.** Hydrothermal features on the floor of Toro crater (17.0°E; 289.2°N) in HiRISE image

606   PSP_005842_1970 (courtesy of NASA/JPL/U of A). A) Small-scale mounds on the floor of

607   Toro crater, marked by white arrows. B) Polygonal pattern on the floor of Toro crater.

608 **10.** Oblique view of the ice dome in Korolev crater (~80km diameter). View is from the rim at

609   72.9°N, 162.6°E looking to the east. The elevation data used for this view are MOLA gridded

610   data and the height of the dome from the trough is ~1 km. CTX images used:

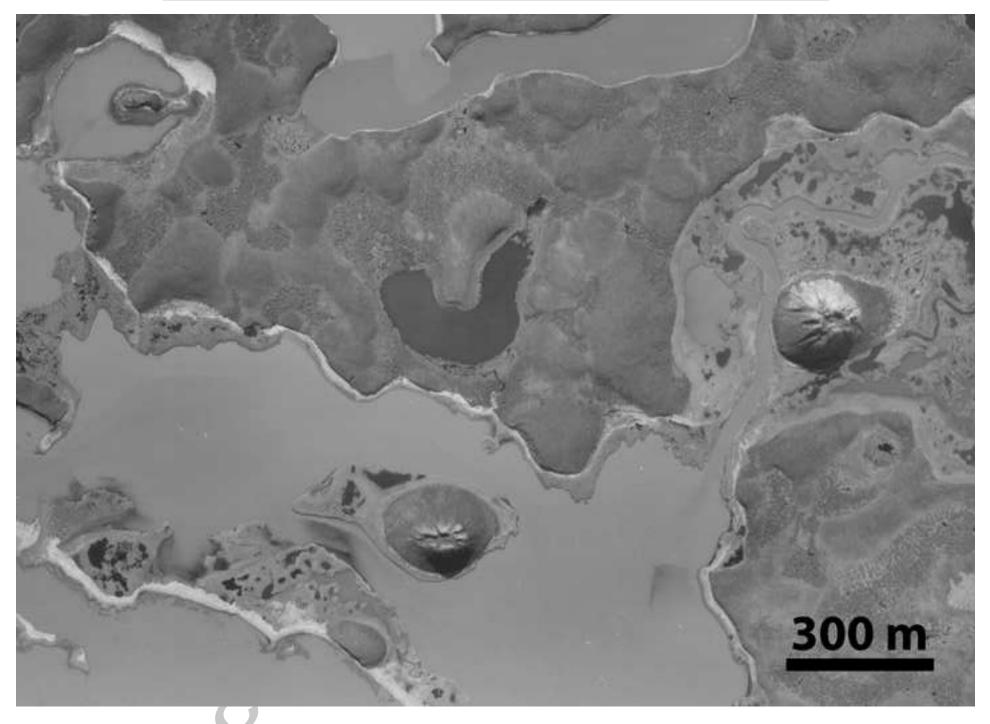611   P21_009042_2528 and P20_008831_2529 (courtesy of MSSS/Caltech/JPL).

612

613 **Tables**

614 **Table 1.** Crater floors studied in this article, their locations and the images used. Crater IDs marked with * indicate those craters
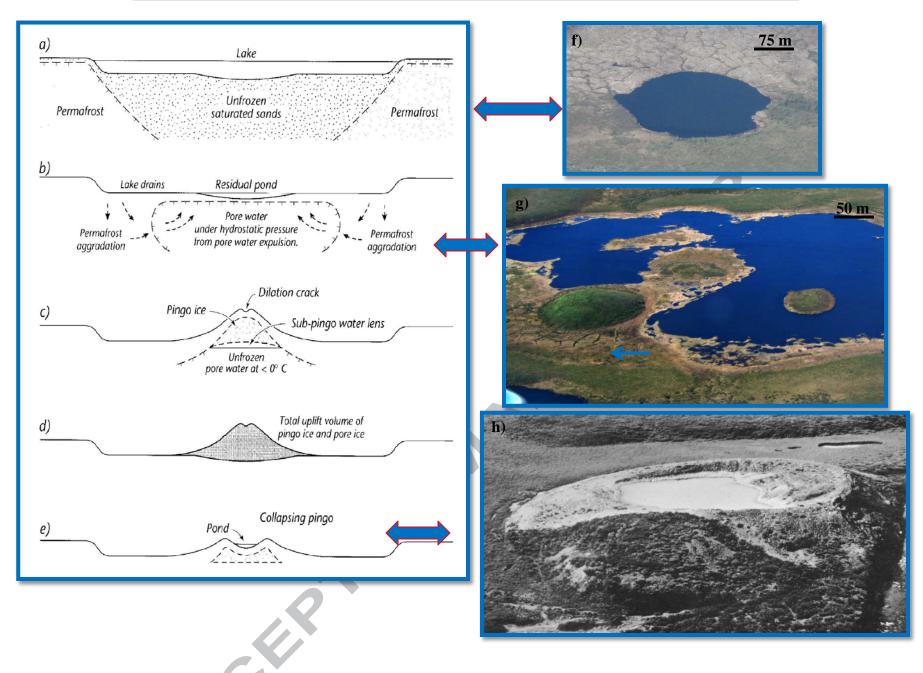
615 included in the Soare et al. (2005) study.

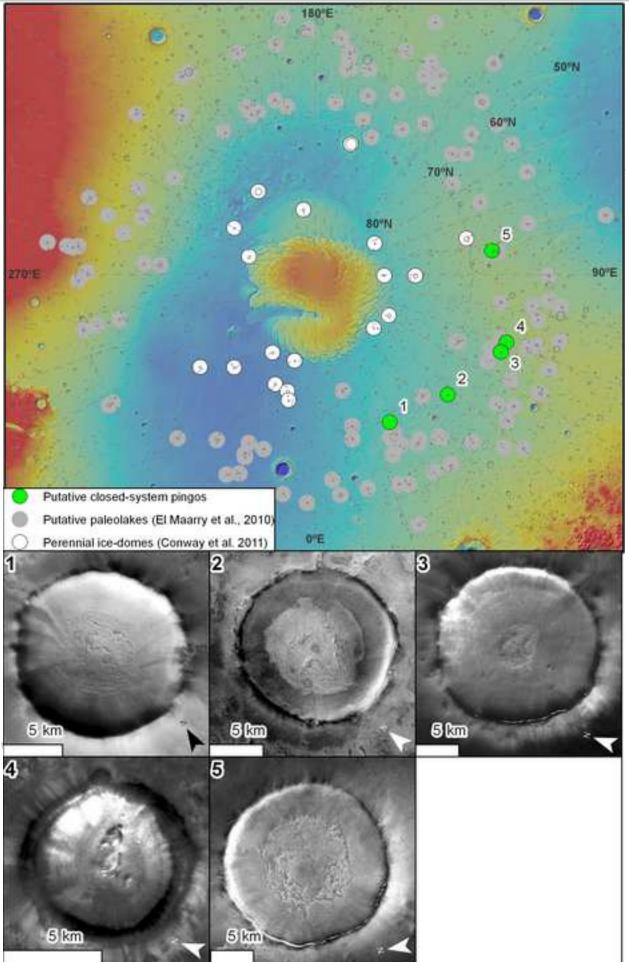| Crater ID	Latitude (°N)	Longitude (°E)	HiRISE images	MOC images	CTX images
1	68.945	26.760	PSP_008757_2490, ESP_017691_2910		B02_010392_2491
2	67.193	47.845	PSP_007372_2475, ESP_017525_2475, ESP_017090_2475		P16_007372_2474
3*	64.476	67.285	PSP_008492_2450, PSP_007780_2450	E0300299	P19_008492_2446
4*	64.324	70.378	ESP_015942_2445, ESP_018210_2445, ESP_018078_2445	E0500113	B22_018078_2445
5	67.131	97.547	ESP_017009_2475, ESP_017154_2475, ESP_017576_2475		B19_017154_2472

616

617 **Table 2.** Characteristics of craters containing mounds and the mounds themselves. Crater-elevation data are taken from MOLA and

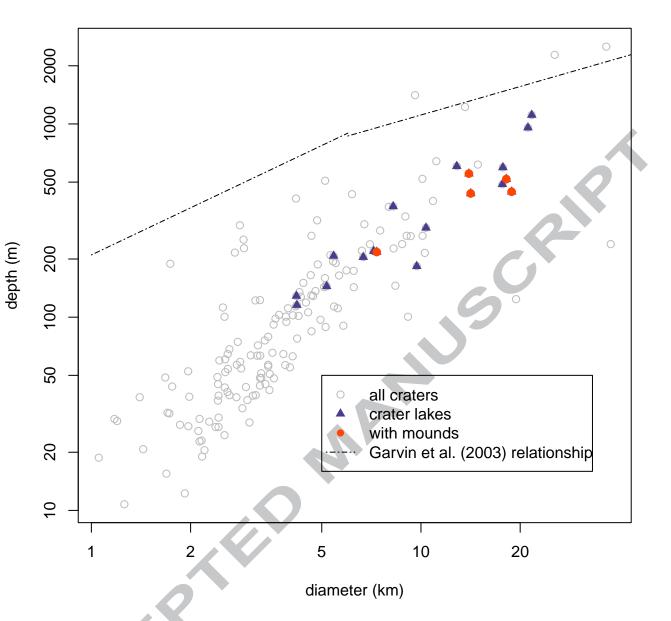618 mound-elevation data are taken from HiRISE stereo-elevation models (cf. supplementary Figure 1).

Crater ID	Depth (m)	Diameter (km)	Predicted depth from Garvin et al. (2003) (m)	Estimated fill thickness (m)	Central uplift height from Garvin et al. (2003) (m)	Estimated elevation difference - central uplift to surface (m)	# of mounds (# used for height measurements)	Aerial extent of mound-basin (km^2)	Mound density (#/km^2)	Mean height in metres (range)	Mean diameter in metres (range)
1	553	14.0	1312	759	154	605	13	30	0.43		
2	437	14.1	1316	879	154	725	44 (16)	51	0.86	15 (6-33)	278 (186-458)
3	518	18.2	1492	974	176	798	36	128	0.28		
4	218	7.3	954	736	110	625	8 (8)	12	0.67	15 (8-22)	194 (86-366)
5	446	18.8	1516	1070	179	891	68	105	0.65		

619

300 m

a) Lake — Permafrost — Unfrozen saturated sands — Permafrost

b) Lake drains — Residual pond — Permafrost aggradation — Pore water under hydrostatic pressure from pore water expulsion. — Permafrost aggradation

c) Dilation crack — Pingo ice — Sub-pingo water lens — Unfrozen pore water at < 0° C

d) Total uplift volume of pingo ice and pore ice

e) Pond — Collapsing pingo

f) 75 m

g) 50 m

h)

Putative closed-system pingos
Putative paleolakes (El Maarry et al., 2010)
Perennial ice-domes (Conway et al. 2011)

Craters in local area to Mounds

CTX
P16_007372_2474

MOLA profile 20037

N

200 m

Initial depth estimate
of crater

5 km

THEMIS
V09919018
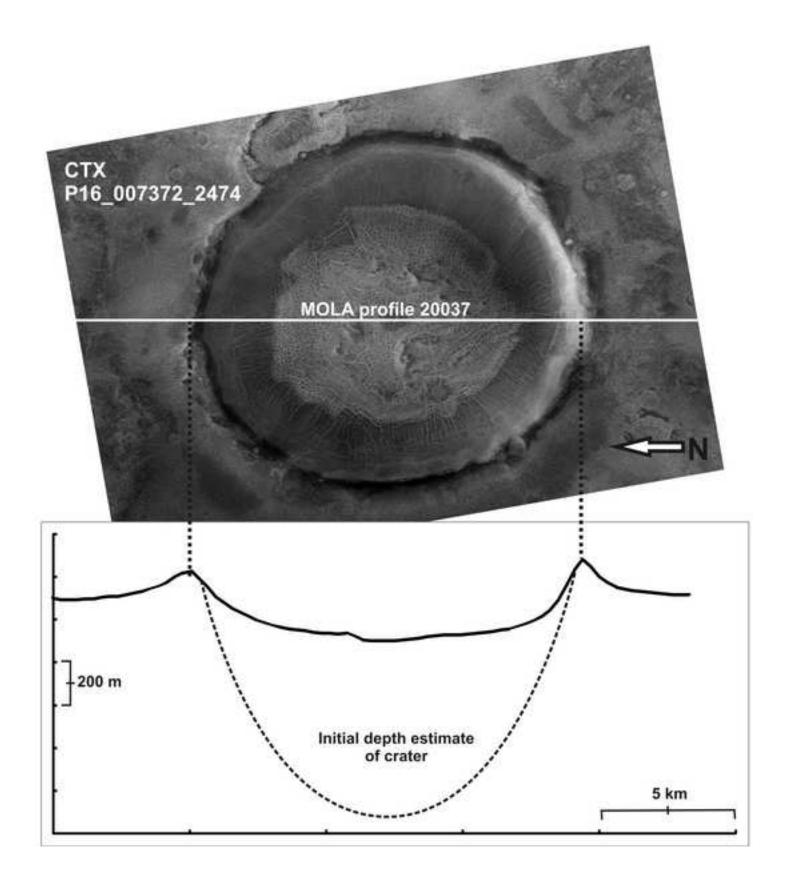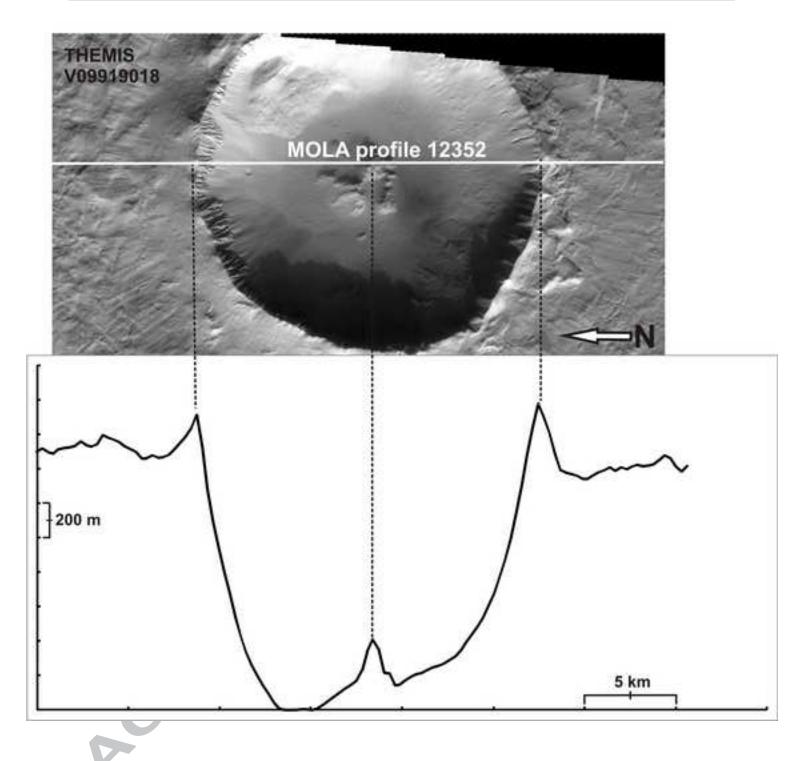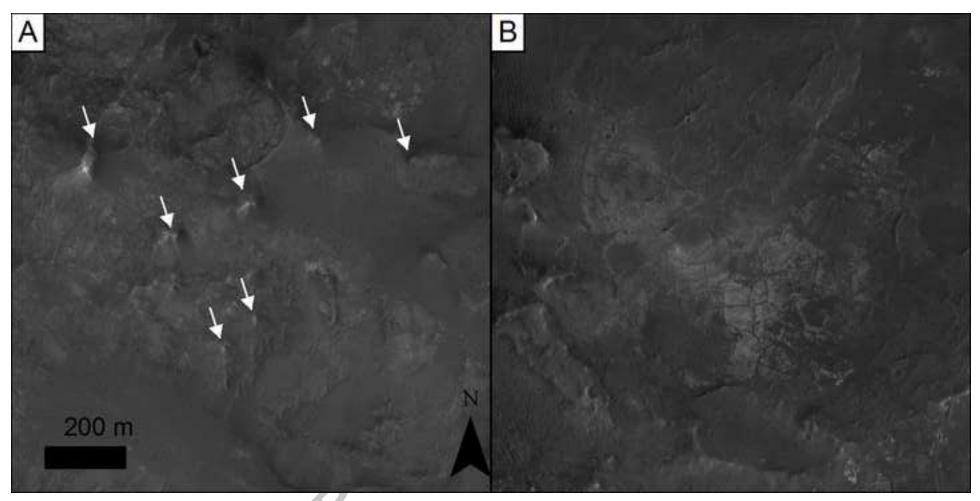
MOLA profile 12352

N

200 m

5 km

621 **Highlights**

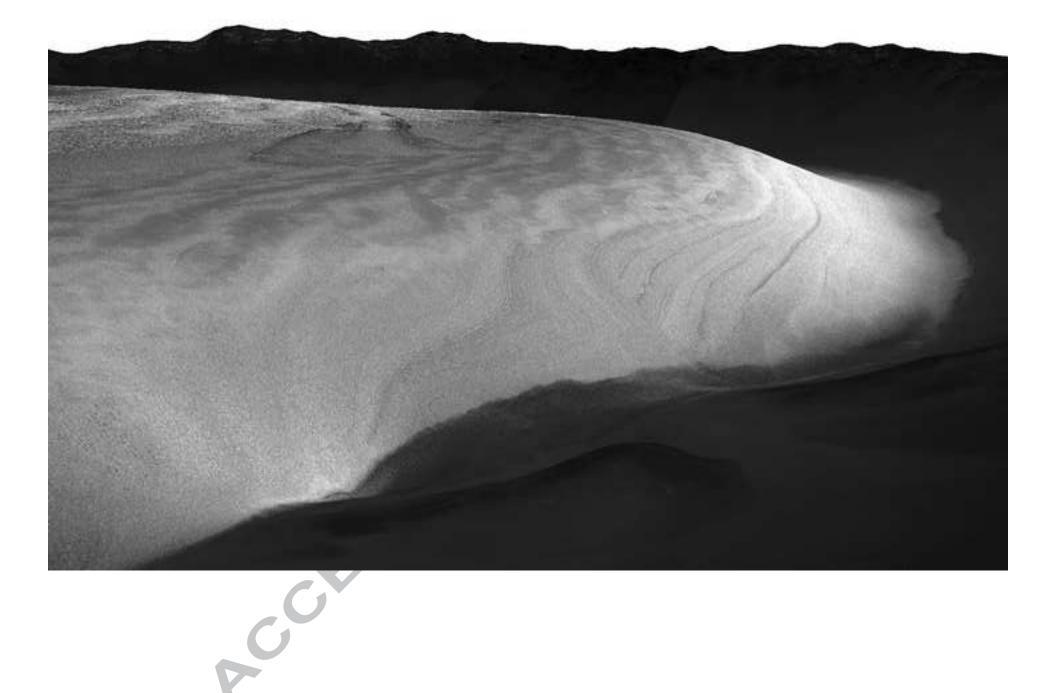622 >Closed-system pingos (CSPs) are perennial ice-cored mounds>They form from pooled surface
623 H_2O and by means of freeze-thaw cycling>Mound-like CSPs occur in 5 highly-filled northern
624 near-polar impact craters on Mars>Formation hypotheses based on leading alternatives are
625 shown to be less robust>CSPs need regional boundary-conditions to be wetter/warmer than most
626 models predict
627
628
629
630